Design and analysis of manufacturable alternating phase-shifting masks

Ron L. Gordon, Chris A. Mack, and John S. Petersen*

FINLE Technologies, Inc., PO Box 162712, Austin, TX 78716
*International SEMATECH, 2706 Montopolis Dr., Austin, TX 78741-6499

ABSTRACT

The advent of mask topography simulation has made possible not only the investigation of the effects of scattering from the mask on the aerial image quality, but also allows a search for mask configurations that produce the desired results. In this work, we first provide studies of the effective phase in a phase-shifting mask by varying both the relative subtractive etch depth in the quartz (corresponding to the Kirchhoff phase difference) and the etch bias (dual trench depth). Ultimately, the sensitivity of the resist linewidth with respect to the effective phase error takes on a critical importance in production, and one may desire to know how to alter a given mask in order to eliminate undesired effects from such errors. A design methodology that takes these issues into account employing a mask topography simulator and a lithography simulator is the end result of this study and is illustrated using an example taken from sub-130 nm lithography.

1. Introduction

The impact of the phase-shifting mask (PSM) on the optical lithography community has been no less than remarkable. As Levenson *et al.* outlined in their first paper on the subject[1], resolution is nearly doubled for sufficiently coherent illumination ($\sigma \lesssim 0.3$). Although the concept of a PSM is easy to grasp, the numerous manufacturing challenges they present are the subject of much active research to this day. We consider here the simplest case of the 2D alternating phase-shifting mask, which is modeled by a π phase in every other space on the mask. This phase shift can be created by a subtractive etch into the quartz mask substrate of every other space, and the etch depth *ED* required for a given phase ϕ is simply

$$ED = \frac{\phi}{2\pi}\frac{\lambda}{(n-1)}, \tag{1}$$

where λ is the wavelength of the light source, ϕ is in radians, and n is the index of refraction of the quartz substrate. With this subtractive etch, there is no risk of material mismatch and the subsequent internal losses that can alter the effective transmission of the shifted region for additive process[2]. Unfortunately, the subtractive process may introduce other problems, such as linewidth variation and CD placement error[3].

As illustrated in several papers[4], the root cause of these problems is an aerial image intensity imbalance in the shifted and unshifted regions. The most immediate fix to this imbalance is the addition of a dual trench[5]; for example, alternating phases of π and 2π instead of 0 and π, respectively. While the dual trench has been shown to improve matters in the image plane, it can also introduce other problems, such as a decrease in image log-slope[5]. Therefore, other fabrication techniques, such as symmetric and asymmetric undercut etching, wet etching, and perturbing the width of the shifted space, have been proposed to improve the image plane intensity distribution[6].

With all the advances made in this area, there still remain many challenges to the design of a simple, manufacturable phase-shifting mask. We note that the treatment of the topographic effects in these phase-shifting masks would not be possible without the introduction of software that simulates the rigorous scattering effects as predicted by the Maxwell equations. Each topography simulation, resulting in a complex mask transmission function, typically takes much more computer resources than the typical aerial image computation. A computing paradigm is therefore sought that minimizes the number of rigorous computations necessary in order to optimize a PSM over the design space that may be of concern to the manufacturer.

This paper represents a first step in this direction. By using the 2D mask topography simulation program ProMAX[7] together with the aerial image simulation of PROLITH/2 v6.0, we consider the effect of a PSM not only in the image plane, but also through focus. In the interest of simplicity, we will only vary the dual trench etch depth and the phase shift etch depth; other degrees of freedom will be considered in later work[8]. As will be seen in Section 2, the dual trench introduces a phase error into the mask that destroys the intensity balance out of focus that it achieved in focus. A method is proposed for quantifying this effective phase error by defining the focus offset between adjacent spaces. It turns out that such phase error can be modeled separately using simple imaging theory, and an analytical approximate expression for this error is given in Section 3. We work through the optimization process in Section 4; here, it becomes clear that the merging of the more rigorous electromagnetic simulation and the approximate diffraction theory results in a computational procedure that is much improved over a simple search over both parameters. Section 5 contains a summary of our findings and recommendations for future work.

2. Impact of Phase Errors in a PSM on the Aerial Image

Before assessing the problems faced with the standard PSM and its dual-trenched variations, it is worthwhile to review what is expected out of a typical PSM from simple diffraction theory. For example, we desire to print 100 nm lines with a 2:1 duty cycle. Our 4X stepper has DUV illumination (248 nm wavelength), a numerical aperture of 0.6, and partial coherence factor of 0.31. The resulting aerial image is shown in Figure 1. Of course, this image was generated using the Kirchhoff approximation for the mask transmission function; that is, the mask is represented by a constant (complex) transmission in each space, and a zero for each line.

Improved simulation accuracy comes with taking the effects of electromagnetic scattering from the mask features (topography) into account. In order to proceed with this computation, we need information about the mask materials and the polarization of the incident light. Here, we will assume that the lines are chrome with an index of $0.85 + i\,2.01$ and these lines sit on a quartz substrate of index 1.51. Further, we will assume that the illumination is E-polarized; that is, the electric field is oriented parallel to the lines in the mask. This information will be used in a mask topography simulator, which solves the Maxwell equations in the region about the mask[7]. The output of such a simulator can be a complex transmission function sampled immediately below the mask, and this function can be the input to an aerial image simulator.

The results of such a computation for the basic PSM are illustrated in Fig. 2(a), and the intensity imbalance discussed above is clear here. In Fig. 2(b), we show the intensity balancing effect of a dual trench (corresponding to a global phase bias of π radians). While the intensity balance is still not perfect, and the reduction in log-slope may pose a problem, it seems that the problems associated with the intensity imbalance are almost solved with this simple design.

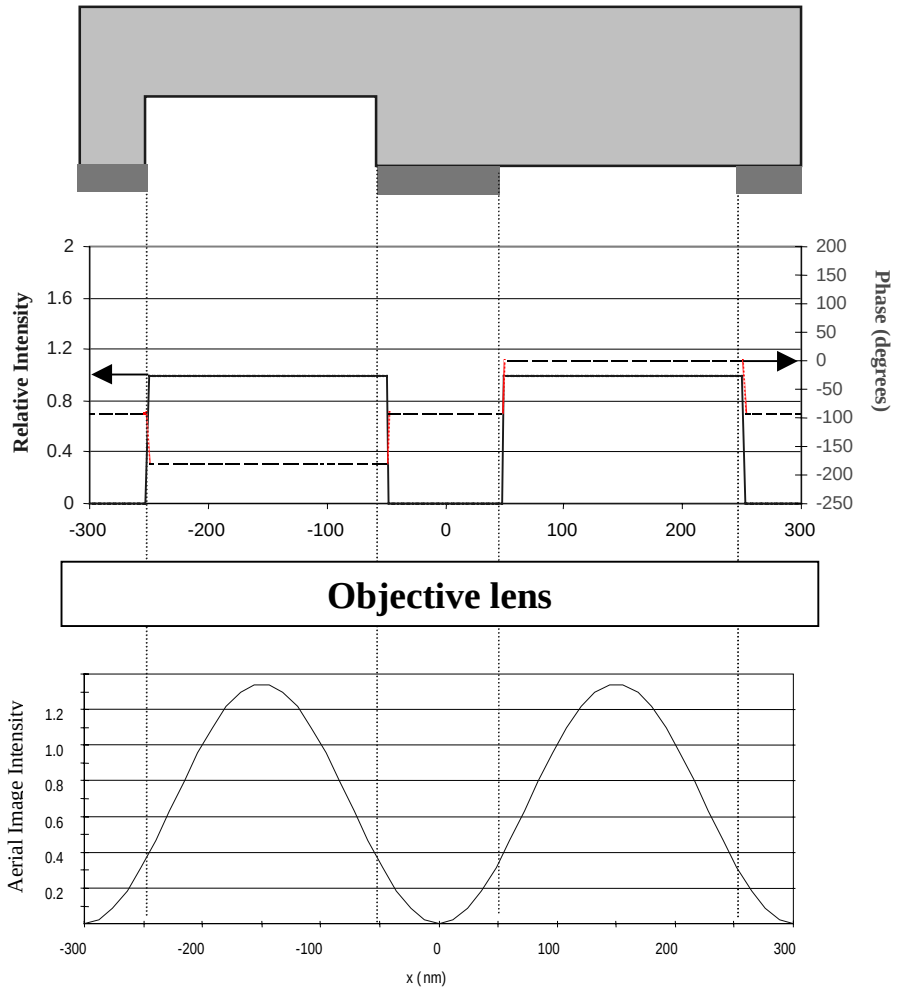

Figure 1. The Kirchhoff transmission function and, upon being imaged by an objective lens, the corresponding in-focus aerial image intensity from a perfect PSM.

So far, we have only looked at a single focal plane. We must consider many planes through focus in order to assess the useful behavior of an aerial image. Figure 3 illustrates the problem that faces us: once we go out of focus, the intensity balance achieved with this dual trench is destroyed. This intensity imbalance is due to different best foci for each space. The fact that the shifted and unshifted intensities have different behaviors through focus points to an effective phase error in the mask. It is this phase error that we shall now study in more detail.

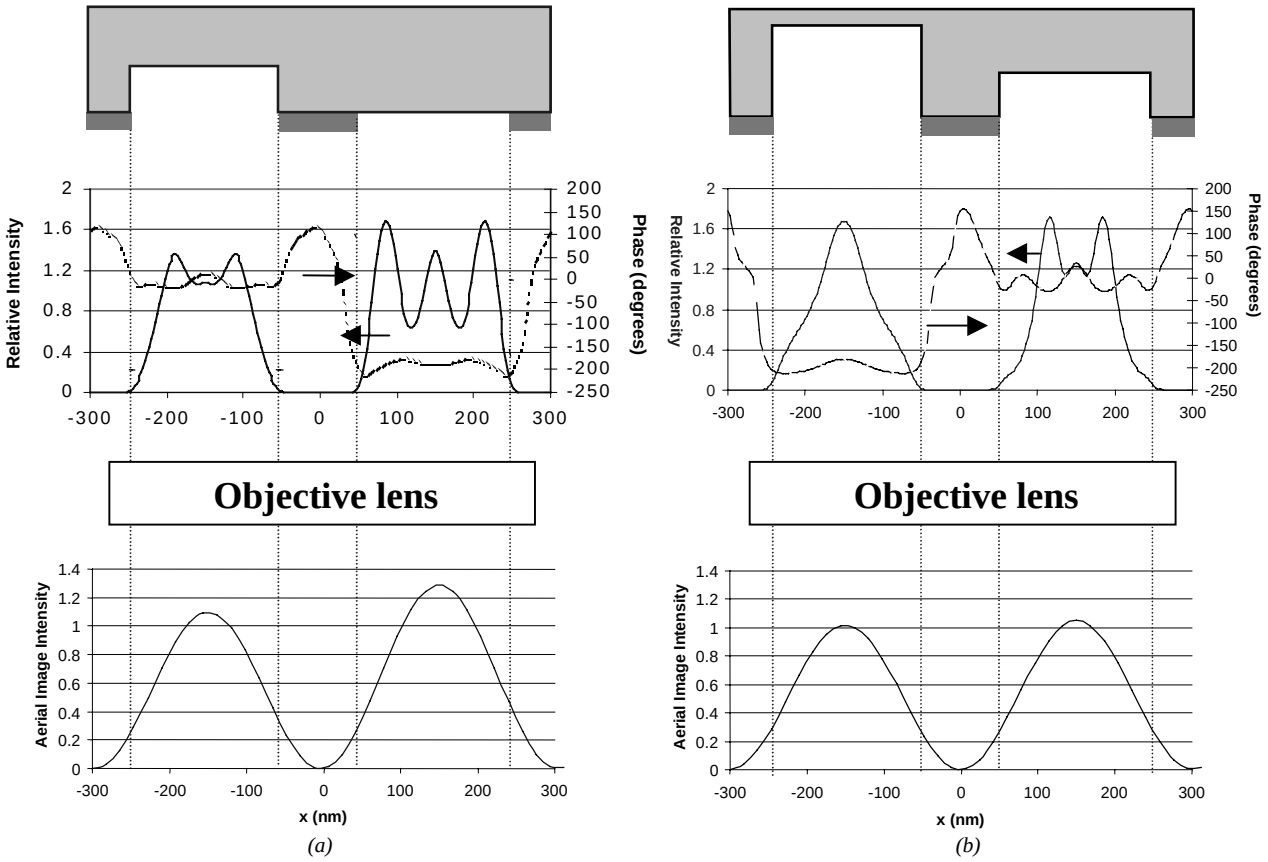

Figure 2. The field immediately below the mask, and the in-focus aerial image intensity resulting from imaging through the projection lens, taking the scattering effects from the mask topography into account: (a) For a simple subtractive alternating PSM, and (b) using a dual trench corresponding to a global phase bias of π radians.

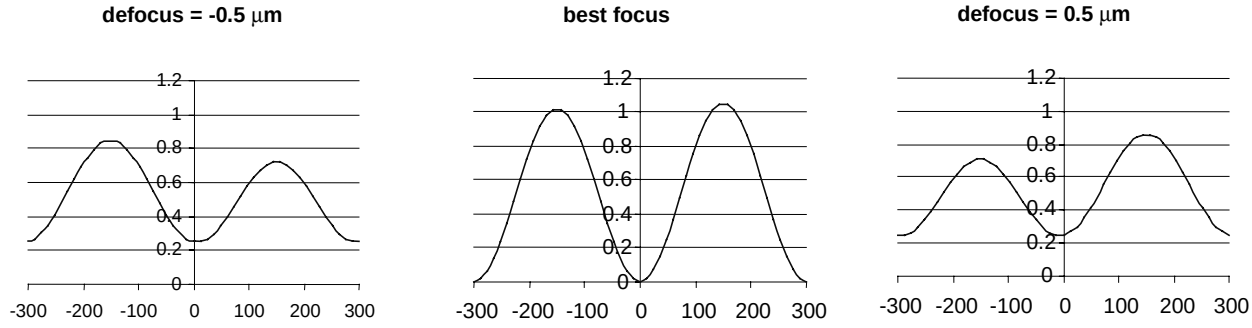

Figure 3. Aerial images for the dual trench setup, as in Figure 2(b), but for various values of defocus. The center plot is identical to that in Figure 2(b).

The simplest way to visualize the impact of phase error on the aerial image is to go back to the Kirchhoff thin-mask model. Looking again at Figs. 2 and 3, we see that the intensity peaks under the shifted and unshifted spaces form the basis of our evaluation of the quality of the behavior of the PSM at a particular

value of defocus. It is then of interest to trace the behavior of these peaks through all values of defocus that are of interest (we will go between $\pm 0.5\mu$m of defocus). This is done in Fig. 4, where these traces are performed for a perfect PSM (ϕ = 180º) and a PSM with a small phase error (ϕ = 170º). With this picture, the effect of the phase error becomes clear: it causes the planes of best focus of the shifted and unshifted spaces to be offset from one another[9]. This offset will be denoted by Δz and will be called the *focus offset* of the adjacent spaces on the mask.

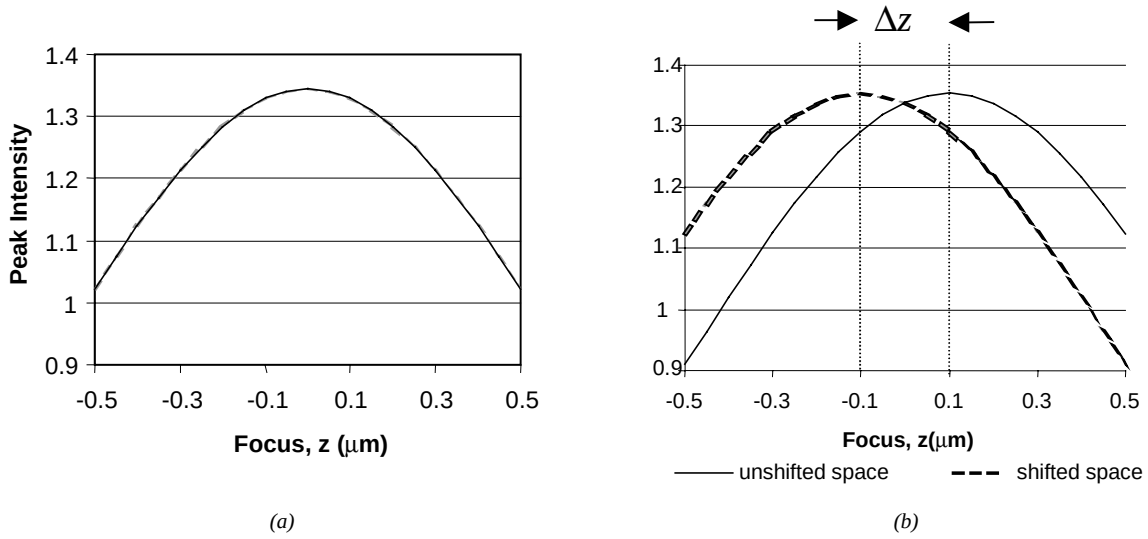

(a) *(b)*

Figure 4. Traces of the intensity peaks for shifted and unshifted spaces for (a) $\phi = 180^\circ$, and (b) $\phi = 170^\circ$ for thin-mask (i.e., Kirchhoff) calculations.

A similar picture is provided in Fig. 5, but taking into account the topography of the mask. Although there are problems present here that are not seen in Fig. 4. – intensity imbalance, intensity reduction, and asymmetry about the intended focus - we will nevertheless describe this result as an effective phase error. By decoupling the focus offset from the topography effects in this manner, we then make it possible to partially replace a complicated scattering model with relatively simple thin-mask model.

In order to optimize the PSM, it is necessary to quantify the focus offset. Looking at the plots in Figs. 4 and 5, we note that the curves look parabolic. Also, noting that the curve in Fig. 4(a) representing the behavior of the perfect PSM is symmetric with respect to the origin, it is plausible that the phase error only causes a shift in the position of the parabolas. However, it is not obvious how the phase error is related to the peaks of these parabolas. The relationship between these two quantities is of central importance here, and the rest of this work is devoted to finding and utilizing that relationship.

We began by using the computation procedure outlined in the previous section for a variety of dual trench and phase shift etch depths. For each point in the sample space (that is, value of dual trench and phase shift etch depths), curves of the aerial image as a function of defocus in the centers of the shifted and unshifted spaces were generated in PROLITH/2. These curves were then fit to parabolas and the positions of the maxima determined. These best-fit parabolas were the basis for computing the focus offset for the aerial images.

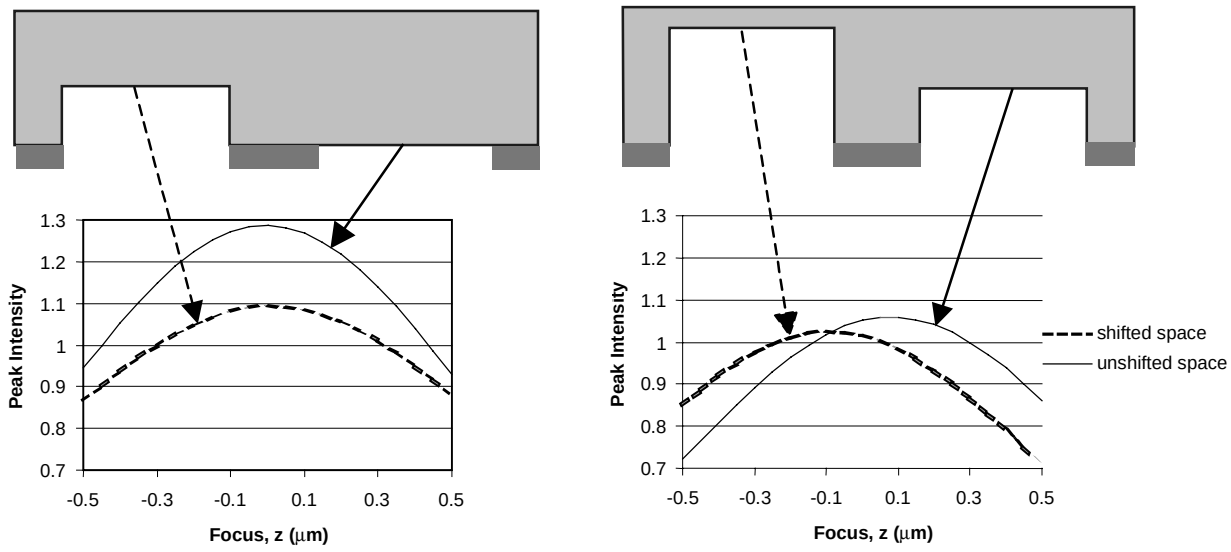

(a) *(b)*

Figure 5 The trace of peak image intensity through defocus for the masks illustrated in Fig. 2. (a) no dual trench, and (b) dual trench.

The results of the simulations are shown in Fig. 6, where the values of the phase shift phase depth run between 0.94π and 1.06π radians (corresponding to phase shift etch depths between approximately 228 nm and 257 nm). Here, the dual trench phase depths take the values 0, $\pi/2$, π, and $3\pi/2$ radians. From these plots, it is clear that there is indeed a linear relationship between focus offset and phase error (that is, deviation of the phase shift phase depth from π radians).

More remarkable, however, is the fact that the values of the slopes of the best-fit lines for each set of data within a given dual trench do not vary much with dual trench depth. Because the dual trench is one of the features of the mask that must be modeled with a full electromagnetic simulation, it follows from this apparent independence from dual trench depth that this focus offset can, in principle, be predicted using the Kirchhoff thin-mask theory. Such a prediction serves two purposes: it provides us with an independent cross-check on the numerical simulation we have been using, and, as will be seen below, it can be used as a roadmap to get us to a desired design more quickly.

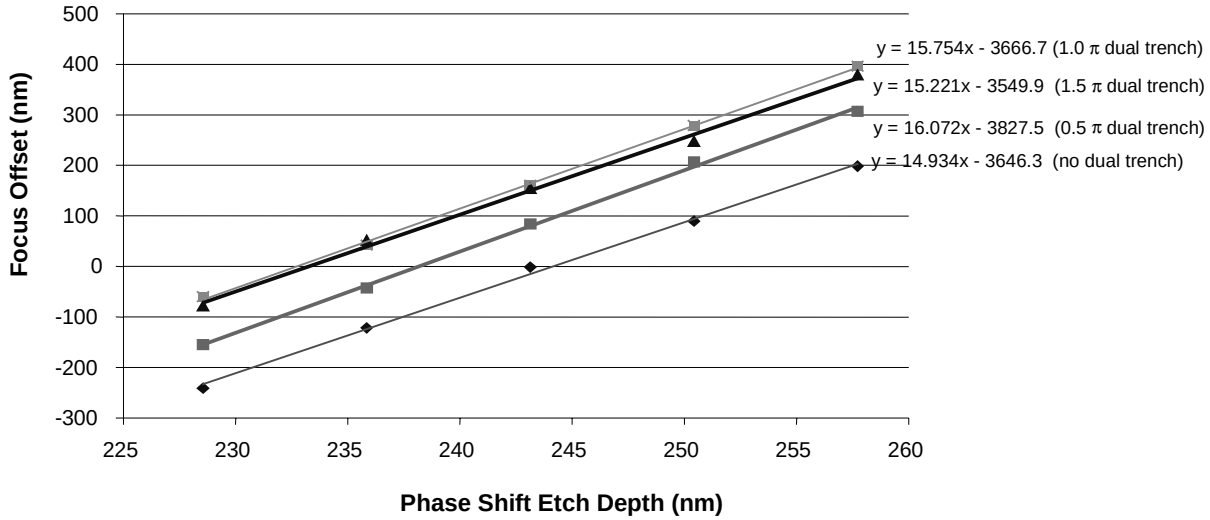

Figure 6. Focus offsets for phase shift phase depths between 0.94π and 1.06π, and dual trench phase depths of 0, π/2, π, and 3π/2.

3. The Thin-Mask Model

We have, in fact, made an approximate prediction for the slope $\Delta ED/\Delta z$ in terms of the mask and imaging data:

$$\frac{\Delta ED}{\Delta z}=\frac{NA^2\sigma^2}{\pi(n-1)}\left(1+\frac{1}{r}\right)\cos\left(\frac{\pi}{2}\frac{1}{r+1}\right)\left[1-\left(\frac{\lambda}{pR}\right)^2\right]^{1/4}\left[1-\left(\frac{\lambda}{p}\right)^2\right]^{-5/4}\left[1+\sqrt{1-\left(\frac{\lambda}{p}\right)^2}\right], \tag{2}$$

where NA is the numerical aperture, σ is the partial coherence factor, p is the full period of the line pattern (which is twice the pitch in this case), r is the duty cycle (ratio of the space width to the line width), and R is the reduction ratio. Again, ED is the phase shift etch depth and Δz is the focus offset. Although a complete derivation of this equation will be presented in a subsequent publication, it is important to understand the conditions under which this expression was derived and, therefore, its ultimate limitations:

1) The phase error $|\varepsilon| \lesssim \pi/10$ radians, so that, for the parameters used here, this implies $|\Delta ED| \lesssim 24\,\text{nm}$.

2) Conventional illumination is used with a partial coherence factor $\sigma \lesssim 0.5$.

3) Only the 0th and 1st diffracted orders pass through the objective lens, and, furthermore, these orders are all contained entirely within the exit pupil (that is, the relation $NA(1-\sigma) \geq \lambda/p$ is satisfied).

The first two assumptions are essential to the derivation, the last is not crucial (although the resulting equation becomes greatly complicated if it is not met). The reason for this is because Eq. (2) was derived using a

scalar model for imaging, where the obliquity factor and complicated defocus behavior do not allow for an analytical evaluation of the integrals involved[10]. Also recall that the ideal PSM has only odd diffracted orders, and we are usually interested in the 1st orders only. The phase error in the PSM introduces small even orders, and we have chosen to neglect any possible 2nd orders that may creep inside the exit pupil of the objective. Again, this approximation is not crucial if the 2nd condition above is satisfied.

It turns out that the mask parameters we are using (specified in Sec. 1) do, in fact, satisfy all of the above conditions. From Eq. (2) and these parameters, we compute that the approximate value of the slope $\Delta z / \Delta ED$ is 14.8, which is within 8% of all the slopes shown in Fig. 6. This close agreement over many values of dual trench depth not only provides a cross-check of our topography results, but, as will be seen in the next section, also allows us to establish an optimization procedure that reduces the number of topography simulations.

4. A Design Paradigm Employing Mask Topography Simulation

While Eq. (2) does not eliminate the need for performing the more computationally intensive rigorous topography modeling, it does lessen the burden of performing the systematic optimizations discussed here. In fact, in combining Eq. (2) and the topography model/aerial image calculations shown, we can define a computational procedure that will allow us to efficiently optimize the mask by eliminating both phase errors and intensity imbalance.

We can perform such an optimization by making the observation that we typically need only a single topography simulation to find the phase shift etch depth that gives zero phase error for a given dual trench etch depth. If, at some given dual trench depth, we perform a topography simulation with some nominal phase shift depth (say, corresponding to π radians), then we can obtain the focus offset through the procedure outlined in Section 2. Because we already know that the focus offset behaves linearly with the phase shift etch depth, and because we already know the slope from Eq. (2), then with knowledge of this focus offset we can compute the etch depth at which no focus offset occurs. We then simulate at this etch depth; if the resulting focus offset is less than some nominal amount (say, 15 nm), then we observe the intensity imbalance. Otherwise, we repeat the last three steps until the focus offset falls below this nominal amount. This process is then repeated for many dual trench etch depths until we have eliminated this intensity imbalance. This process is expressed in a flow chart in Fig. 7.

We have performed such an optimization procedure over several values of dual trench etch depth; the results are illustrated in Fig. 8. Because the dependence of the focus offset on the phase shift depth was far stronger than its dependence on dual trench depth, the grid spacing used in the topography simulation was locked to the phase shift etch depth. The dual trench phase depth can then only be specified within a discrete (small) interval; that interval here was roughly $\pm 0.01\pi$ radians. The values of the dual trench phase depth used here are 0.94π, $0.97\ \pi$, $1.00\ \pi$, $1.03\ \pi$, $1.06\ \pi$, $1.08\ \pi$, $1.10\ \pi$, $1.12\ \pi$, $1.20\ \pi$, $1.30\ \pi$, $1.40\ \pi$, $1.50\ \pi$. Of these depths, we found the best mask to have a dual trench phase depth of $1.10\ \pi$ (etch depth of about 267 nm) and a phase shift phase depth of 0.949π (etch depth of about 231 nm).

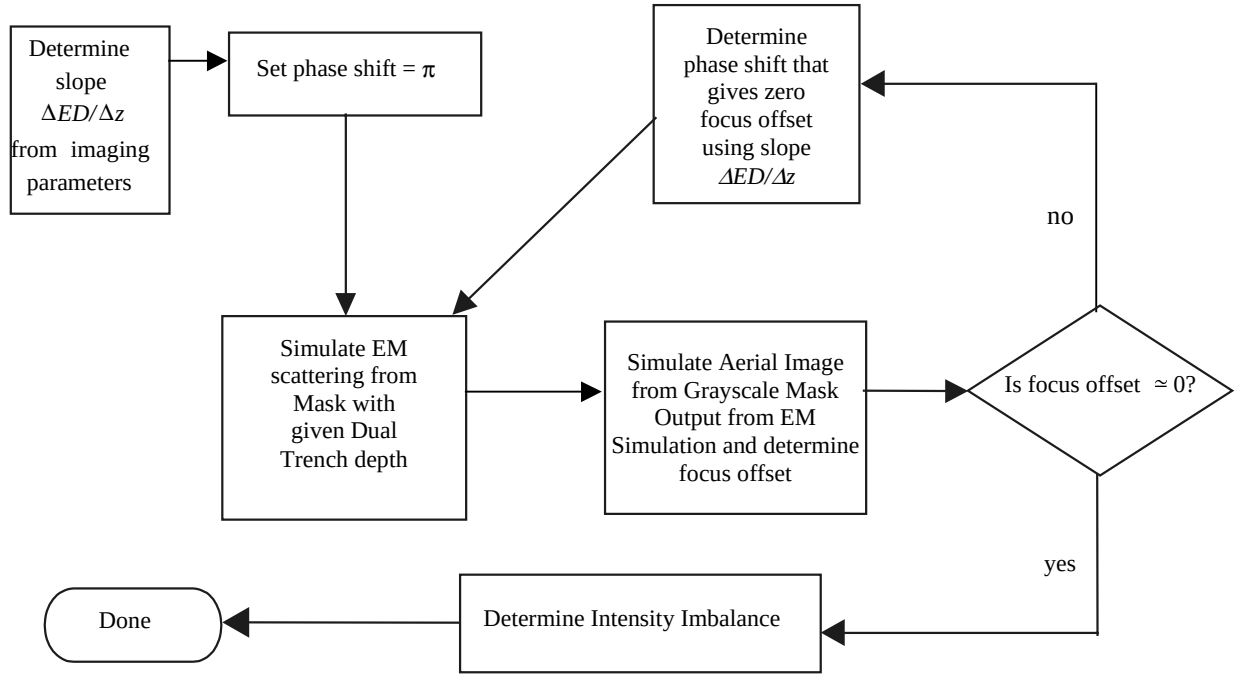

Figure 7. Flow chart for the computational procedure for designing a PSM with no phase error for a given dual trench depth.

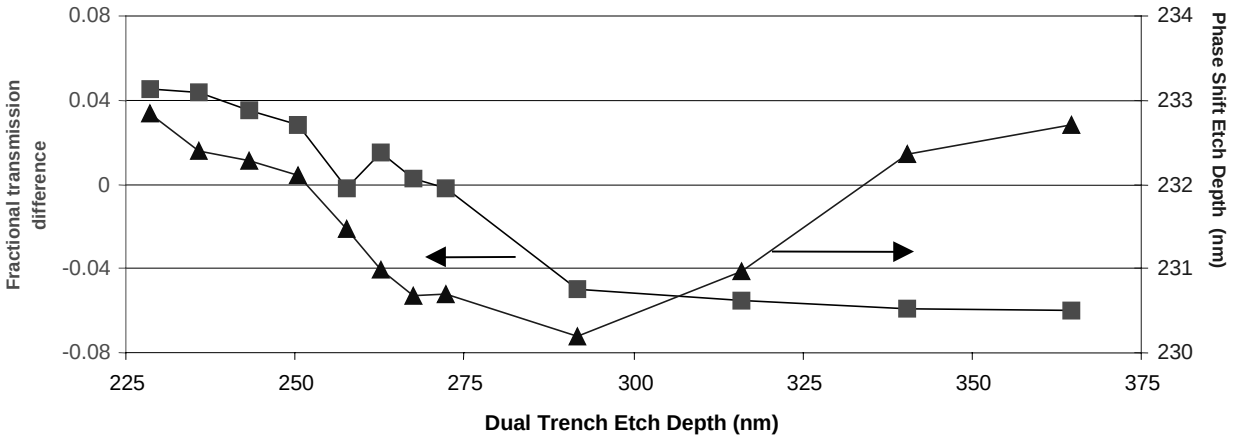

Figure 8. Results of the optimization procedure illustrated in Fig. 7 for the parameters used in the previous figures, and for various dual trench etch depths. The triangle curve represents the phase shift etch depth at each dual trench required to obtain a zero focus offset. The square curve is the corresponding plot of the relative intensity difference between the shifted and unshifted spaces in the mask, sampled at the dual trench and phase shift etch depths specified in the plot. Note that no more than 2 iterations of the procedure outlined in Fig. 7 were necessary here.

Finally, the result of our optimization is presented in Fig. 9. We see here that our goals have indeed been achieved: virtually no phase error or intensity imbalance exist for this mask under the conditions of our simulations.

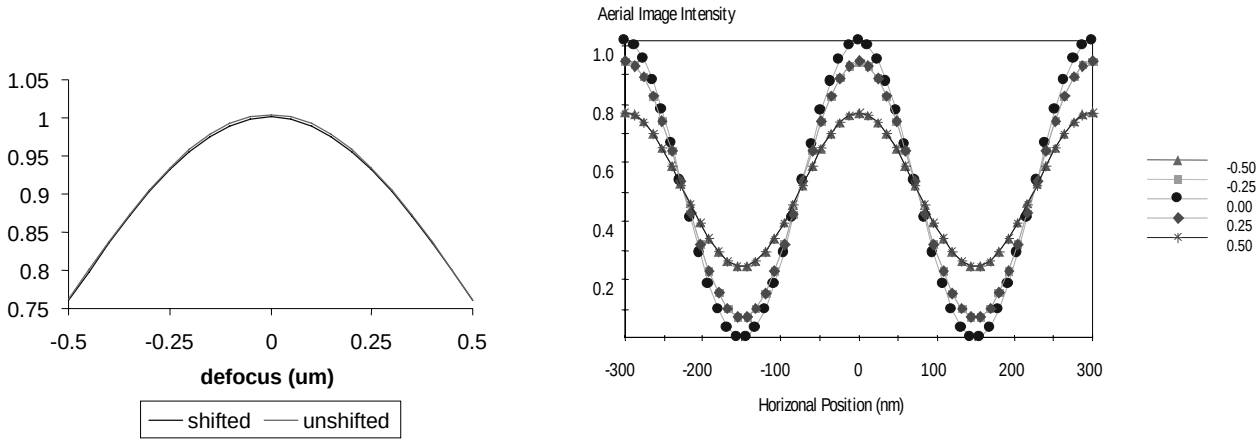

Figure 9 The aerial image intensity distribution for a PSM with a dual trench etch depth of 267 nm and phase shift etch depth of 231 nm: (a) shifted and unshifted intensity peaks through focus, and (b) intensity patterns for various values of defocus.

5. Concluding Remarks

The main results of this work are the method outlined for quantifying the focus offset and the optimization procedure detailed in Fig. 7. The result in Eq. (2) is helpful in reducing the number of topography simulations required to find the optimal mask. The use of this equation in the optimization procedure is the end result of an observation that the phase error in a PSM could be separated from the topography effects (i.e., the slope was almost independent of dual trench depth). The optimization procedure was performed for a particular set of parameters that may occur in the printing of 100 nm lines, and, for this set of parameters, an optimal phase shift and dual trench etch depth was found.

Also, it is seen in comparing Fig. 1 and Fig. 9 that the image log-slope (or image contrast) has been reduced somewhat for the optimized mask. An additional model that adds another degree of freedom - undercuts, for example – in order to improve this contrast will then take on a special interest.

Finally, it should be emphasized that the computations carried out here were performed assuming E-polarized light. An immediate extension of this work uses unpolarized light, and these computations are presently being carried out. Preliminary results for H-polarization indicate a significantly different optimum mask may be found for this case.

This work, however, represents only the beginning of a move to accurately model and design extensions of optical lithography to 100 nm and beyond. One obvious extension of this work will be performed in the lab, where the masks suggested by the results here – and similar results of this optimization for different parameters – are manufactured and tested.

References

[1] M.D. Levenson, N.S. Viswanathan, and R.A. Simpson, "Improving Resolution with a Phase-Shifting Mask", *IEEE Trans. Elect. Dev.* **ED-29**, 1828-1836 (1982).

[2] R.L. Kostelak, C. Pierrat, J.G. Garofalo, and S. Vaidya, "Exposure characteristics of alternate aperture phase-shifting masks fabricated using a subtractive process", *J. Vac. Sci. Tech.* **B10**, 3055-3061 (1992).
[3] J.S. Petersen, *et al.*, "Designing dual-trench alternating phase-shift masks for 140 nm and smaller features using 248 nm KrF and 193 nm ArF lithography", *BACUS News: Photomask*, **14**, Issue 8 (Aug. 1998).
[4] See Ref. 3 for simulation results using METRO (K.D. Lucas, C.M. Yuan, and A.J. Stroljwas, "A rigorous and practical vector model for phase shifting masks in optical lithography", *Proc. SPIE* **1674**, 252-263 (1992). More detailed results are seen in C. Pierrat, A. Wong, S. Vaidya, and M. Vernon, "Phase-Shifting Mask Topography Effects and Lithographic Image Quality", *Proc. SPIE* **1927**, 28-41 (1993).
[5] T. Terasawa, N. Hasegawa, A. Imai, and S. Okazaki, "Analysis of Nonplanar Topography Effects of Phase Shift Masks on Imaging Characteristics", *Japanese J. Appl. Phys.* **34**, 6578-6583 (1995).
[6] R.A. Ferguson, A.K. Wong, T.A. Brunner, and L.W. Liebmann, "Pattern-Dependent Correction of Mask Topography Effects for Alternating Phase-Shifting Masks", *Proc. SPIE* **2440**, 349-360 (1995).
[7] R. Gordon and C.A. Mack, "Lithography simulation employing rigorous solutions to Maxwell's equations", *Proc. SPIE* **3334**, 176-196 (1998).
[8] See Ref. 5 for a study involving optimization over dual trench and back etch depth.
[9] This effect can be seen in T. Teresawa, N. Hasegawa, T. Tanaka, S. Katagiri, and T. Kurosaki, "Improved Resolution of an *i*-line stepper using a phase-shift mask", *J. Vac. Sci. Tech.* **B8**, 1300-1308 (1990).
[10] By using a model that neglects this obliquity factor and using a quadratic phase approximation for defocus, an analytical expression for the intensity can be derived, so long as the assumptions concerning Eq. (2) are true. For more information on these diffraction models, see C.A. Mack, *Inside PROLITH*, Austin: FINLE Technologies, Inc., 1997.